Nonequilibrium relaxation of soft responsive colloids

José López-Molina ; Sebastien Groh ; Joachim Dzubiella ✉ ; Arturo Moncho-Jordá
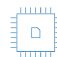
Check for updates

View Online

Export Citation

Nonequilibrium relaxation of soft responsive colloids

View Online   Export Citation   CrossMark

José López-Molina,[1] (ID) Sebastien Groh,[2] (ID) Joachim Dzubiella,[2,3,a)] (ID) and Arturo Moncho-Jordá[1,4,b)] (ID)

AFFILIATIONS

[1] Department of Applied Physics, University of Granada, Campus Fuentenueva S/N, 18071 Granada, Spain
[2] Physikalisches Institut, Albert-Ludwigs-Universität Freiburg, Hermann-Herder Straße 3, D-79104 Freiburg, Germany
[3] Cluster of Excellence livMatS @ FIT—Freiburg Center for Interactive Materials and Bioinspired Technologies, Albert-Ludwigs-Universität Freiburg, D-79110 Freiburg, Germany
[4] Institute Carlos I for Theoretical and Computational Physics, University de Granada, Campus Fuentenueva S/N, 18071 Granada, Spain

a)Author to whom correspondence should be addressed: joachim.dzubiella@physik.uni-freiburg.de
b)Electronic mail: moncho@ugr.es

ABSTRACT

Stimuli-responsive macromolecules display large conformational changes during their dynamics, sometimes switching between states. Such a multi-stability is useful for the development of soft functional materials. Here, we introduce a mean-field dynamical density functional theory for a model of responsive colloids to study the nonequilibrium dynamics of a colloidal dispersion in time-dependent external fields, with a focus on the coupling of translational and conformational dynamics during their relaxation. Specifically, we consider soft Gaussian particles with a bimodal size distribution between two confining walls with time-dependent (switching-on and off) external gravitational and osmotic fields. We find a rich relaxation behavior of the systems in excellent agreement with particle-based Brownian dynamics computer simulations. In particular, we find time-asymmetric relaxations of integrated observables (wall pressures, mean size, and liquid center-of-mass) for activation/deactivation of external potentials, respectively, which are tunable by the ratio of translational and conformational diffusion time scales. Our work thus paves the way for studying the nonequilibrium relaxation dynamics of complex soft matter with multiple degrees of freedom and hierarchical relaxations.

I. INTRODUCTION

Responsive systems have garnered considerable interest in the realm of soft matter science due to their dynamic nature and the ability to adapt to external stimuli.[1] These systems, comprising responsive colloids and macromolecules, exhibit remarkable adaptability, controlling their properties—such as the internal conformation of the particle,[2–5] size,[6–11] shape,[8,12–19] charge density,[8,20] electric dipole,[21] and orientation[22–24]—in response to environmental changes. Such responsiveness, originating from their internal degrees of freedom (DoFs), allows for a nuanced interaction with surrounding particles and external fields, leading to significant alterations in their internal and collective dynamical properties,[1,10,21,25–33] even leading to multi-relaxation time scales.[34]

An important system of RCs is the one for which the particle size (that could represent the radius of gyration of a linear polymer coil,[6,35] or the diameter of a microgel particle[8,36–42]) is the internal property that couples to the center of mass translational degrees of freedom: particles not only move, but also are able to swell/shrink in response to external stimuli such as changes in the solvent pH, salt concentration, and temperature.[43–47] In addition, particle concentration can also provoke the squeezing of the particles, leading to interpenetration, deformation, and compression.[48,49] Precise control over the interplay between size localization and dynamics is paramount for achieving targeted functionality at specific locations and rates. Notable examples are the local modulation of uptake and release kinetics in soft polymer-based nanocarriers, such as microgels for local control of catalysis[50–52] or drug release.[53–57]

Our understanding of soft colloids has been significantly enhanced through developments in equilibrium Density Functional Theory (DFT), which has provided a solid framework for studying

the structure and phase behavior of soft materials under external potentials.[58–62] Classical DFT has been successfully extended to explicitly include varying particle size as a dynamic variable, describing how microscopic interactions and external potentials affect the equilibrium properties of these systems and enabling the exploration of size-dependent phenomena within polydisperse systems.[6,63–65] Recently, we have demonstrated explicitly for a model of responsive colloids (RC)s with size polydispersity[7,9–11] how to employ DFT functionals (in RC-DFT) to study and control the localization of the (size) property in space by external fields.[66,67] However, many interesting behaviors of responsive systems occur out of equilibrium. The dynamical nature of these systems is not only a testament to their adaptability but also to their potential in real applications. In this context, dynamical density functional theory (DDFT) serves as a powerful tool for exploring non-equilibrium processes by modeling the time evolution of the particle density distribution, $\rho(\mathbf{r}, t)$, driven by diffusive, overdamped Brownian dynamics in the presence of external fields and particle interactions.[68–71] The theory can also be modified to incorporate reactions or switching.[72–75] Crucially, it leverages the adiabatic approximation, assuming that the correlations in a non-equilibrium state are akin to those in equilibrium.[68] This theory adapts the equilibrium concepts of DFT to non-equilibrium scenarios, predicting how responsive systems evolve over time. In contrast to conventional polydisperse systems,[63,64] internal degrees of freedom are also able to change during the nonequilibrium process. A systematic study on the coupled dynamics of translation and internal dynamics in the relaxation of a colloidal system as well as the appropriate DDFT is still missing in the literature.

In this work, we present an extension of classical DDFT to responsive systems (denoted by RC-DDFT) that allows us to efficiently investigate the dynamical relaxation in the presence of coupled DoFs under applied external potentials. In particular, we consider soft responsive colloids (RCs), for which the size of the particles (σ) changes in response to the interactions with the rest of particles or with an applied external potential. This external potential depends on the position and also the size of the particle, i.e., $u_{\text{ext}}(\mathbf{r}, \sigma)$, making the colloidal system inhomogeneous in terms of position and size. In addition to the external potential, this system of responsive colloids also requires the knowledge of the free energy landscape for the particle size, $\psi(\sigma) = -kT \ln p(\sigma)$ (where $p(\sigma)$ represents the parent size-distribution of a single RC), which acts as an additional external potential controlling the size fluctuations.[11] Here, we focus on a system formed by bistable particles for which $p(\sigma)$ is described by a generic Landau-like bimodal size distribution[76,77] so that the particle size fluctuates between two states (big and small) separated by an energy barrier. This particular two-state behavior is relevant in the conformation of many biological or functional macromolecules, such as folded/unfolded or globule/coil transitions of proteins and polymers.[5,31,78–82] For this system, we analyze the time evolution of the one-body density profile, $\rho(\mathbf{r}, \sigma; t)$, after sudden activation/deactivation of the external field, and explore the non-equilibrium transient dynamics resulting from the interplay between structural relaxation and size relaxation.

This paper is organized as follows: In Sec. II, we describe the main statistical mechanics equations, discuss DFT, and generalize its dynamical counterpart to deal with non-equilibrium systems

of responsive colloids under external potentials (RC-DDFT). We also introduce in this section a mean field model for soft Gaussian colloids with a bimodal distribution of states. Brownian dynamic simulations of RCs are explained in Sec. III. Section IV presents the results and discussion of the non-equilibrium dynamics of RCs under the activation/deactivation non-equilibrium processes for two representative external potentials: gravitation and osmotic. We specially focus on investigating the appearance of non-equilibrium transient dynamics states that arise due to the interplay between translational diffusion and particle swelling/shrinking. Finally, in Sec. V, we present the main conclusions of our work.

II. THEORETICAL BACKGROUND

A. Theoretical modeling of responsive colloids (RCs)

In the following, we briefly recall the most basic statistical relations between distributions and averages for the RC model.[11,67] As common in the theory of liquids, we assume a (isotropic) distance-dependent pair potential for the RC liquid. For RCs, however, the particle–particle pair potential not only depends on the positions $\mathbf{r}_i$ and $\mathbf{r}_j$ of both particles i and j, but also has an explicit dependence on the size of both interacting particles, σ_i and σ_j, that is $u(|\mathbf{r}_i - \mathbf{r}_j|, \sigma_i, \sigma_j)$. The external potential can be expressed as $u_{\text{ext}}(\mathbf{r}_i, \sigma_i)$. Hence, the total potential energy of N responsive particles can be expressed as

$$U = \sum_i \psi(\sigma_i) + \frac{1}{2} \sum_i \sum_{j \neq i} u(|\mathbf{r}_i - \mathbf{r}_j|, \sigma_i, \sigma_j) + \sum_i u_{\text{ext}}(\mathbf{r}_i, \sigma_i), \quad (1)$$

where ψ is the energy landscape for the size σ of an isolated particle. The inhomogeneous properties of an RC fluid immersed in an external potential are fully described by the particle density distribution, $\rho(\mathbf{r}, \sigma)$,[11,67] defined in such a way that integration over the four coordinates (three translational ones and the size) provides the total number of particles in the system,

$$\int_V d\mathbf{r} \int d\sigma \rho(\mathbf{r}, \sigma) = N, \quad (2)$$

so $\rho(\mathbf{r}, \sigma)$ is measured in units of length^{-4}.

In the limit of very low particle concentrations and negligible external potential, the one-body density converges to $\lim_{\rho_0 \to 0} \lim_{u_{\text{ext}} \to 0} \rho(\mathbf{r}, \sigma) = \rho_0 p(\sigma)$, where $\rho_0 = N/V$ is the bulk particle density and $p(\sigma)$ is the so-called *parent* distribution, defined as the size distribution of a single isolated responsive particle that does not interact with external forces or with other particles, which is normalized to unity, $\int p(\sigma) d\sigma = 1$. We can express $p(\sigma)$ in terms of the free energy landscape as

$$p(\sigma) = p_0 e^{-\beta \psi(\sigma)}, \quad (3)$$

where $\beta = 1/(k_B T)$ (T is the absolute temperature and k_B is the Boltzmann constant) and p_0 is a constant prefactor to fulfill the normalization of $p(\sigma)$. For higher particle concentrations or in the presence of external fields, the single-particle property distribution will change: We denote by $f(\sigma) = N(\sigma)/N$ the *emergent* probability distribution, where $N(\sigma)d\sigma$ is the number of particles with an internal property within $[\sigma, \sigma + d\sigma]$ in the system and N is the total number of particles. In particular, in the absence of any

external field, the one-body particle density may be expressed as $\lim_{u_{ext} \to 0} \rho(\mathbf{r}, \sigma) = \rho_0 f(\sigma)$.

B. Dynamical density functional theory for RCs

1. Equilibrium DFT prerequisites

Let us recall first the treatment of the RC model in the framework of equilibrium DFT. The inhomogeneous free energy functional of a RC fluid immersed in the external potential $u_{ext}(\mathbf{r}, \sigma)$ is given by[11,63,67]

$$
\begin{aligned}
F[\rho(\mathbf{r}, \sigma)] = k_B T \int d\mathbf{r} \int d\sigma \rho(\mathbf{r}, \sigma) \big[\ln \left(\rho(\mathbf{r}, \sigma) \Lambda^3 / p_0 \right) - 1 \big] \\
+ \int d\mathbf{r} \int d\sigma \rho(\mathbf{r}, \sigma) [u_{ext}(\mathbf{r}, \sigma) + \psi(\sigma)] \\
+ F_{ex}[\rho(\mathbf{r}, \sigma)],
\end{aligned} \tag{4}
$$

where $\Lambda = h/(2\pi m k_B T)^{1/2}$ is the thermal wavelength. The first term of Eq. (4) is the ideal gas free-energy functional. The second term takes into account the interaction of the RC fluid with the external potential. Note that $\psi(\sigma)$ also plays the role of an external potential for the particle size, i.e., it represents the energy cost implied in the swelling/shrinking of each responsive colloid. Finally, the third contribution is the excess free energy of the fluid that arises due to the existence of particle–particle interactions.

The grand canonical potential energy functional of a RC fluid is

$$
\Omega[\rho(\mathbf{r}, \sigma)] = F[\rho(\mathbf{r}, \sigma)] - \mu_0 \int d\mathbf{r} \int d\sigma \rho(\mathbf{r}, \sigma), \tag{5}
$$

where μ_0 is the (constant) chemical potential of the RC fluid. The equilibrium density profile is the one that minimizes the grand canonical functional, $\delta\Omega/\delta\rho(\mathbf{r}, \sigma) = 0$. Applying this functional differentiation to Eq. (5) with Eq. (4) and solving the resulting Euler–Lagrange equation for the particle density $\rho(\mathbf{r}, \sigma)$, we find

$$
\rho(\mathbf{r}, \sigma) = q \exp\left(-\beta\psi(\sigma) - \beta u_{ext}(\mathbf{r}, \sigma) - \beta\mu_{ex}(\mathbf{r}, \sigma) \right), \tag{6}
$$

where $\mu_{ex}(\mathbf{r}, \sigma)$ is the excess chemical potential, given by the functional differentiation of the excess free energy, $\mu_{ex}(\mathbf{r}, \sigma) = \delta F_{ex}/\delta\rho(\mathbf{r}, \sigma)$, and q is a normalization constant that is obtained by imposing conservation of the total number of particles, namely Eq. (2). The solutions of Eqs. (6) and (2) lead to the equilibrium position and size distribution $\rho_{eq}(\mathbf{r}, \sigma)$.

2. Dynamical DFT for a RC fluid

Under non-equilibrium conditions, the one-body density distribution becomes also time-dependent, $\rho(\mathbf{r}, \sigma; t)$. For the case of responsive colloids, particles in the system do not only diffuse in the space, but can also modify their size in response to external interactions. To describe their dynamics, we make the assumption that the property σ of each particle also follows an overdamped diffusive dynamics. Following the prescription given in the work by Baul and Dzubiella,[9] we denote D_T as the translational diffusion coefficient and D_σ as the diffusion coefficient in the σ-space. It is important to emphasize that D_T depends in general on the particle size (as for Stokes–Einstein), so $D_T(\sigma)$ is a function of σ.

The DDFT can be extended to RCs by defining a four-dimensional vector $\mathbf{x} = (x, y, z, \sigma) \equiv (\mathbf{r}, \sigma)$ and a four-dimensional

current $\mathbf{J} = (J_x, J_y, J_z, J_\sigma) \equiv (\mathbf{J_r}, J_\sigma)$ (note that this current has dimensions of length^{-3}time^{-1}). Analogously, we can write a four-component *nabla* operator $\nabla_\mathbf{x} = (\partial/\partial x, \partial/\partial y, \partial/\partial z, \partial/\partial\sigma) \equiv (\nabla_\mathbf{r}, \nabla_\sigma)$. The time evolution of the density profile is given by

$$
\frac{\partial \rho(\mathbf{x}, t)}{\partial t} = -\nabla_\mathbf{x} \cdot \mathbf{J}(\mathbf{x}, t) = -\nabla_r \cdot \mathbf{J_r} - \frac{\partial J_\sigma}{\partial\sigma}. \tag{7}
$$

The components of the current $\mathbf{J}$ are

$$
\begin{cases}
\mathbf{J_r} = -D_T(\sigma)\rho(\mathbf{r}, \sigma; t)\nabla_\mathbf{r}[\beta\mu(\mathbf{r}, \sigma; t)], \\
J_\sigma = -D_\sigma\rho(\mathbf{r}, \sigma; t)\dfrac{\partial\beta\mu(\mathbf{r}, \sigma; t)}{\partial\sigma},
\end{cases} \tag{8}
$$

where $\mu(\mathbf{r}, \sigma; t)$ is the non-equilibrium chemical potential. In order to calculate it, we make use of the adiabatic approximation and assume that $\mu(\mathbf{r}, \sigma; t)$ is given by the functional derivative of the equilibrium free energy functional, $\mu = \delta F/\delta\rho$. Using Eq. (4), it leads to[66]

$$
\begin{aligned}
\mu(\mathbf{r}, \sigma; t) = k_B T \ln\left(\rho(\mathbf{r}, \sigma; t)\Lambda^3/p_0 \right) + u_{ext}(\mathbf{r}, \sigma) + \psi(\sigma) \\
+ \mu_{ex}(\mathbf{r}, \sigma; t),
\end{aligned} \tag{9}
$$

where $\mu_{ex} = \delta F_{ex}/\delta\rho$. Equations (7)–(9) define the new generalized dynamical density functional theory designed for responsive colloids (RC-DDFT).

C. Mean-field responsive DDFT of soft Gaussian responsive colloids confined in planar slits

Here, we specify our particular system of responsive colloids and the corresponding excess free energy model for it to be used in the RC-DDFT framework. In this work, we focus on systems composed by soft interpenetrable RCs. We consider the following size-dependent Gaussian-core pair potential for the particle–particle interaction:

$$
\beta u(|\mathbf{r} - \mathbf{r}'|, \sigma, \sigma') = \varepsilon \exp\left(-4|\mathbf{r} - \mathbf{r}'|^2/(\sigma + \sigma')^2 \right), \tag{10}
$$

where $\varepsilon > 0$ is the (repulsive) interaction strength (in $k_B T$ units), which we assume to be independent of the particle sizes. It represents an estimate of the particle hardness: for small values of ε, colloids are able to interpenetrate each other. On the contrary, large values of ε correspond to harder colloids, for which the energy penalty of overlapping is very high. Here, $(\sigma + \sigma')/2$ plays the role of the interaction range. In fact, in this interaction model, σ represents the effective diameter of each RC.

The Gaussian-core interaction model is a well-established coarse-grained description of polymer solutions,[83] as it has been shown to accurately describe the interaction between two isolated polymers immersed in a good solvent, for polymer of identical[84] and different lengths,[85] under both homogeneous and the inhomogeneous conditions.[86] For different choices of the interaction parameters, one can obtain either a mixture exhibiting bulk fluid–fluid (macro)phase separation[70,87–89] similarly to polymer blends, or alternatively, a mixture exhibiting microphase separation.[90]

We assume that $\varepsilon = 2$ (in $k_B T$ units) for the interparticle interaction strength. This value represents fairly well the soft repulsion existing between linear polymers.[86,88] The equilibrium properties

of such soft Gaussian particles described by Eq. (10) are well represented by a weakly correlated mean-field fluid over a surprisingly wide density and temperature range.[86] This justifies the use of the mean-field approximation for the excess free-energy of the interacting RC fluid, given by

$$F_{\text{ex}} = \frac{1}{2} \iint_V d\mathbf{r} d\mathbf{r}' \iint d\sigma d\sigma' \rho(\mathbf{r}, \sigma) \rho(\mathbf{r}', \sigma') u(|\mathbf{r} - \mathbf{r}'|, \sigma, \sigma'). \quad (11)$$

This approximation has been successfully used to reproduce the equilibrium and non-equilibrium properties of passive[89,91] and active switching Gaussian colloids.[73–75]

Performing the functional differentiation and introducing it into Eq. (9) leads to the explicit expression for the non-equilibrium chemical potential of a mean-field RC fluid,

$$\mu(\mathbf{r}, \sigma; t) = k_B T \ln \left(\rho(\mathbf{r}, \sigma; t) \Lambda^3 / p_0 \right) + u_{\text{ext}}(\mathbf{r}, \sigma) + \psi(\sigma)$$
$$+ \int d\mathbf{r}' \int d\sigma' \rho(\mathbf{r}', \sigma'; t) u(|\mathbf{r} - \mathbf{r}'|, \sigma, \sigma'), \quad (12)$$

which involves a convolution integral in the $\mathbf{r}$ coordinate.

In our work, we consider RC dispersions confined between two parallel hard walls separated by a distance L and subjected to one-dimensional external potentials, $u_{\text{ext}}(z, \sigma)$, where $z \in [0, L]$ is the distance from the left wall. The rest of the coordinates are assumed to run over the full range, $x, y \in]-\infty, \infty[$ (infinite slit). In this case, the density profiles are homogeneous in lateral directions and can be expressed as $\rho(\mathbf{r}, \sigma; t) = \rho(z, \sigma; t)$, with the normalization

$$\int_0^L dz \int d\sigma \rho(z, \sigma; t) = N/S, \quad (13)$$

where N/S is the prefixed number density per area S and the normalization is valid for every time t.

Exploiting the planar symmetry to simplify the convolution integral involved in Eq. (12), we find the following equation for the non-equilibrium chemical potential:[66]

$$\mu(z, \sigma; t) = k_B T \ln \left(\rho(z, \sigma; t) \Lambda^3 / p_0 \right) + u_{ext}(z, \sigma) + \psi(\sigma)$$
$$+ \frac{\pi \varepsilon}{4} \int d\sigma' (\sigma + \sigma')^2 \int_0^L dz' \rho(z', \sigma'; t) e^{-\frac{4(z-z')^2}{(\sigma+\sigma')^2}}. \quad (14)$$

In addition to the interparticle interaction potential, we need to specify the parent distribution of the RC, $p(\sigma)$. In this work, we consider bistable particles, for which the size fluctuates between two states of size σ_1 and σ_2, which can be referred to as small and big, respectively. This implies considering a bimodal parent size distribution, with both peaks centered around these two states. To model this behavior, we choose a generic bimodal form using a symmetric double-Gaussian function,

$$p(\sigma) = \frac{p_0}{2\sqrt{2\pi\tau^2}} \left[\exp\left(-\frac{(\sigma - \sigma_1)^2}{2\tau^2}\right) + \exp\left(-\frac{(\sigma - \sigma_2)^2}{2\tau^2}\right) \right] \quad (15)$$

with $\sigma_1 = 0.63\sigma_0$ and $\sigma_2 = 1.37\sigma_0$ (σ_0 represents a reference particle size that will be used as a unit length for the rest of the sizes and distances). In order to avoid nonphysical negative values and extremely large values of the particle size, the range of σ has been limited to be $\sigma \in [0.1\sigma_0, 2\sigma_0]$.

The parameter τ appearing in Eq. (15) provides the thickness of the size distribution around both peaks and can be interpreted as the particle softness (conversely, τ^{-1} represents the stiffness of the RC). In this work, we use $\tau = 0.2\sigma_0$. With this choice, the free energy barrier required to overcome to switch from one state to other is $\Delta\psi \approx 1k_B T$.

In our system, the σ-dependence of the translational diffusion coefficient will be of the type of Stokes, $D_{\text{T}}(\sigma) = D_0\sigma_0/\sigma$, where D_0 is the diffusion coefficient of a particle of radius σ_0. In addition, a parameter α is introduced to control the ratio between σ-diffusion and translational diffusion, $D_\sigma = \alpha D_0$. We also define our diffusion time for either translation or size relaxation as $\tau_{\text{B}} = \sigma_0^2/D_0$.

From $\rho(z, \sigma; t)$ and integrating over the σ-coordinate, we obtain the one-body number density distribution of the RC fluid in our quasi-1D system, namely

$$\rho(z; t) = \int d\sigma \rho(z, \sigma; t). \quad (16)$$

The position-dependent size distribution of the RC fluid at time t and position $\mathbf{r}$, $f(\mathbf{r}, \sigma; t)$, is obtained as[66]

$$f(\mathbf{r}, \sigma; t) = \frac{\rho(\mathbf{r}, \sigma; t)}{\rho(\mathbf{r}; t)}. \quad (17)$$

We analyze some representative integrated properties and monitor their time evolution: The center of mass location of the RC fluid is given by

$$\langle z(t) \rangle = \frac{S}{N} \int_0^L z dz \int d\sigma \rho(z, \sigma; t). \quad (18)$$

The mean size of the RC at position z is given by the normalized first moment of the distribution,

$$\langle \sigma(z; t) \rangle = \frac{1}{\rho(z; t)} \int d\sigma \rho(z, \sigma; t) \sigma. \quad (19)$$

The (global) mean size of the RC is given by

$$\langle \sigma(t) \rangle = \frac{S}{N} \int_0^L dz \int d\sigma \rho(z, \sigma; t) \sigma. \quad (20)$$

In our work, we assume that the confining walls are ideal planar hard walls. Thus, the colloids experience an infinite repulsion when their center of mass is located at $z = 0$ and $z = L$, respectively. For these ideal walls, the average (osmotic) pressure exerted on the left and right walls is given, respectively, by[61]

$$P_{\text{left}}(t) = \rho(0; t) k_B T \quad \text{and} \quad P_{\text{right}}(t) = \rho(L; t) k_B T. \quad (21)$$

III. BROWNIAN DYNAMICS SIMULATIONS OF RCs

Brownian dynamics (BD) calculations are performed in the framework of the RC model.[11] The discretized form of the BD equations for the translational degrees of freedom and for the internal property is given by

$$\begin{cases} \mathbf{r}_i(t + \Delta t) = \mathbf{r}_i(t) + \frac{D_{\text{T}}}{k_B T} \mathbf{F}_{\text{T}}^{(i)}(t) \Delta t + \boldsymbol{\xi}_{\text{T}}, \\ \sigma_i(t + \Delta t) = \sigma_i(t) + \frac{D_\sigma}{k_B T} F_\sigma^{(i)}(t) \Delta t + \xi_\sigma, \end{cases} \quad (22)$$
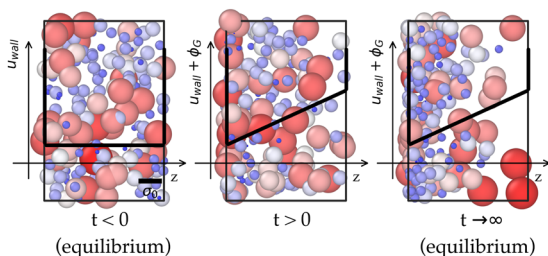
FIG. 1. Representative snapshots of system configurations made of responsive colloids obtained at different times from Brownian dynamics simulations. For $t < 0$, the system is in equilibrium with hard walls on the left and on the right (solid line). At $t = 0$, the system is perturbed by switching on ϕ_G (solid line) and relaxes (for $t > 0$) before reaching the new equilibrium at $t \to \infty$ (solid line). The color gradient from blue (small sizes) to red (large sizes) visualizes the magnitude of the sizes of the colloids.

where Δt is the simulation time step. While $\mathbf{F}_T^{(i)}(t)$ $= -\nabla_{r_i} u_{ext}(\sigma_i, z; t) - \sum_{j \neq i}^N \nabla_{r_i} u(\mathbf{r}_i - \mathbf{r}_j, \sigma_i, \sigma_j)$ is the translational force acting on colloid i from both the external field and the pairwise interactions with the other colloids, $F_\sigma^{(i)}(t)$ $= -\nabla_{\sigma_i} \psi(\sigma_i) - \nabla_{\sigma_i} u_{ext}(\sigma_i, z; t) - \sum_{j \neq i}^N \nabla_{\sigma_i} u(\mathbf{r}_i - \mathbf{r}_j, \sigma_i, \sigma_j)$ is the property force acting on colloid i resulting from its own free-energy landscape $\psi(\sigma)$ and its interaction with both the external field and the pairwise interactions with the other colloids. Finally, $\boldsymbol{\xi}_T$ and ξ_σ are random vector and random scalar, respectively. Both $\boldsymbol{\xi}_T$ and ξ_σ are drawn from a normal distribution with zero mean and variance $\langle \xi_{T,\alpha} \xi_{T,\beta} \rangle = 2 D_T \Delta t \delta_{\alpha\beta}$ and $\langle \xi_\sigma^2 \rangle = 2 D_\sigma \Delta t$, respectively, with $\alpha, \beta = x, y, z$ being the Cartesian components and $\delta_{\alpha\beta}$ being the Kronecker delta function.

Simulations were performed using the same geometry and potential parameters as the ones used in RC-DDFT. To avoid nonvanishing, non-physical negative values, and extremely large values of the colloid size, the range of σ was limited to $[0.1, 2]\sigma_0$ by simply rejecting (Monte Carlo like) moves that would lead to $\sigma < 0.1\sigma_0$ or $\sigma > 2\sigma_0$. The same procedure was used to respect the hard walls. Starting with an equilibrium configuration made of 432 responsive colloids [see Fig. 1(a)], the system was perturbed by either abruptly switching on or off the applied external potential, prior to a relaxation run of $30\tau_B$ during which the system reached a new equilibrium state [see Fig. 1(c)]. To obtain the time-dependent density, $\rho(z; t)$, and mean size, $\langle \sigma(t) \rangle$, $N_{run} = 4000$ independent runs were performed. The density profile and the mean size were then averaged over all configurations for a fixed time t.

IV. RESULTS AND DISCUSSION

For our non-equilibrium relaxation study, our methodology consists in applying an external potential,

$$u_{ext}(z; \sigma; t) = u_{walls}(z) + \phi(z, \sigma; t), \qquad (23)$$

where u_{walls} accounts for the confinement effects and ϕ represents an additional external interaction such as osmotic or

gravitational potentials, defined further below. In particular, the wall potential is

$$u_{walls}(z) = \begin{cases} 0 & \text{for} \quad 0 \leq z \leq L, \\ \infty & \text{for} \quad z < 0 \quad \text{or} \quad z > L. \end{cases} \qquad (24)$$

We initiate our system at equilibrium and consider two time-dependent protocols. In the first one, the external potential ϕ is absent for $t < 0$ and is activated for $t > 0$ (*switch on*) to observe the ensuing relaxation toward the new equilibrium state (reached in the limit $t \to \infty$) (cf. Fig. 1 as a representative illustration). In the second protocol, we follow the inverse process: the field is already activated for $t < 0$, and it is *switched off* for $t > 0$. A comparison between both procedures will allow us to examine whether the system shows a different relaxation dynamics during the switching on and switching off processes.

This bidirectional exploration is conducted for two external potentials, namely gravitational (ϕ_G) and osmotic (ϕ_O) potentials:

(i) The gravitational external potential is linear in "height" z and reads as

$$\phi_G(z) = Az \qquad \text{for} \quad 0 \leq z \leq L, \qquad (25)$$

with $\beta A \sigma_0 = 1$. Note that the gravitational potential is just a function of position z, not of size. Still, density inhomogeneities will also affect the compressible particle sizes and their distributions in time and space. A relatively quick activation of this external field can be experimentally implemented in several ways. For instance, the system could be confined within a very narrow cell that is suddenly rotated to align with the gravitational field. Alternatively, the cell can be vigorously shaken to ensure a homogeneous distribution of particles before aligning with the gravitational field. In a zero-G airplane experiments, a gravitational field would in principle be also switched off and on.

(ii) The osmotic potential, $\phi_O(z, \sigma)$, is given by

$$\phi_O(z, \sigma) = Bz\sigma^3 \qquad \text{for} \quad 0 \leq z \leq L, \qquad (26)$$

where $\beta B \sigma_0^4 = 1$. This equation introduces a dependence on particle size through the σ^3-volume term, aiming to replicate the volumetric effects exerted by the osmotic pressure that arises when the colloidal particles are immersed in a suspension of certain cosolutes whose concentration varies spatially with a constant gradient. As such, σ^3 represents the volume excluded by each colloid to the cosolute molecules within this gradient.[6,11] Indeed, if we denote with $\rho_c(z)$ the cosolute concentration at a distance z from the left wall, the osmotic pressure is $\Pi(z) = k_B T [\rho_c(0) - \rho_c(z)]$. For a constant negative concentration gradient, $\rho_c(0) - \rho_c(z) = Cz$ ($C > 0$). The osmotic potential for a spherical colloid that excludes a volume $V = \pi\sigma^3/6$ thus reads as $\phi_O(z, \sigma) = \Pi(z)V = Bz\sigma^3$, where $B = (\pi/6)Ck_B T > 0$.

To validate the theoretical predictions of our extended DDFT, they are compared with BD simulation results. Through this comparison, we analyze macroscopic quantities such as the mean position $\langle z(t) \rangle$, the mean size $\langle \sigma(t) \rangle$, and the pressure exerted on

the hard walls. Moreover, we delve into a parametric study focusing on the interplay between spatial relaxation and size relaxation times, governed by the parameter $\alpha = D_\sigma/D_0$: For $\alpha < 1$, the swelling/deswelling of the responsive colloid is slower than the translational diffusion, which means that the change of particle size happens retarded to the structural relation. The opposite occurs for $\alpha > 1$. This dissimilar time relaxation is expected to lead to transient dynamic states, tunable by α, which will be explored in Sec. IV D.

Figure 1 provides a representative illustration of the activation protocol for the particular case of the gravitational external potential. Big and small particles are depicted as red and blue spheres, respectively. The rest of the intermediate sizes are represented by a continuous graduation of colors between red and blue. At time $t < 0$ (left panel), the responsive system is in the equilibrium state, confined between two planar hard walls. After activation of the external field (central panel) at $t = 0$, particles dynamically relax in the new potential field and migrate toward the left to lower the external potential energy. Their sizes are also affected by the changes in the local particle concentration. For $t \to \infty$ (right panel), the system finally reaches the final equilibrium state in the presence of the external potential, with a very different profile and size distribution compared to the original state.

A. Gravitational potential

We start analyzing the relaxation dynamics of a responsive colloidal system immersed in the gravitational external potential given by Eq. (25) under the two protocols (switching on and off). For this case, we select $\alpha = 0.1$ and $N/S = 1.2\sigma_0^{-2}$. Figure 2 depicts the time evolution of the mean local density $(\rho(z;t))$ and local mean size $(\langle\sigma(z;t)\rangle)$ from $t = 0$ to $3\tau_B$ at $\Delta t = 0.5\tau_B$ intervals. Panels (a) and (c) show the results following the activation ("switch on") of the gravitational field, while panels (b) and (d) depict the outcomes subsequent to its deactivation ("switch off").

The analysis of $\rho(z)$, depicted in Figs. 2(a) and 2(b), reveals a significant alignment between the BD and RC-DDFT methods throughout the dynamic process. These panels also indicate that the system has reached nearly the final equilibrium state already for $t \approx 3\tau_B$. Conversely, the evaluation of $\langle\sigma(z;t)\rangle$ in Figs. 2(c) and 2(d) demonstrates a consistent conformity between the methods, albeit with notable differences, particularly a consistent disparity of ~5% throughout the dynamic sequence. This deviation in $\langle\sigma(z;t)\rangle$ arises not only in this confined geometry but also in bulk systems (without external potentials and walls). We attribute this small discrepancy to the (adiabatic[92] and/or mean-field) approximations employed in RC-DDFT. To facilitate a clearer comparison with simulations by eye, the magnitude of the RC-DDFT values of $\langle\sigma(z;t)\rangle$ in Fig. 2 has been rescaled by a factor of 1.05.

In the initial stage ($t = 0$) of the activation state, depicted in Fig. 2(a), we observe a nearly flat density profile, $\rho(z)$, with the exception of regions near the walls where particle adsorption effects become prominent. This accumulation near the hard walls occurs because particles are pushed from the bulk to the walls due to the
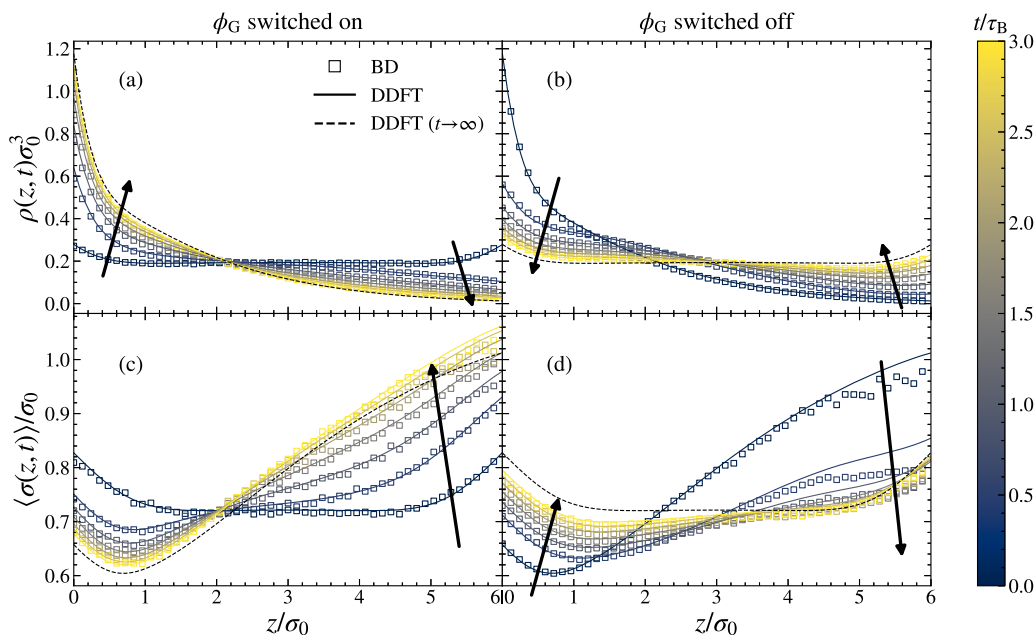

FIG. 2. Time evolution of the density $\rho(z;t)$ and size $\langle\sigma(z;t)\rangle$ of the RCs in the gravitational field, $\phi_G(z)$, plotted at different times ranging from $t = 0$ (dark blue) to $3\tau_B$ (yellow), with a time interval of $\Delta t = 0.5\tau_B$. The lines represent the theoretical predictions obtained with RC-DDFT, whereas the symbols correspond to BD simulations. Panels (a) and (c) show, respectively, the local density $[\rho(z;t)]$ and the local mean size ($\langle\sigma(z;t)\rangle$) obtained when the external potential is switched on for $t > 0$. Similarly, panels (b) and (d) show the same quantities, but for the deactivation process ("switched off"). In this case, the magnitude of $\langle\sigma(z;t)\rangle$ obtained via RC-DDFT is rescaled by a factor of 1.05 for a clearer comparison. All calculations are performed considering $\alpha = 0.1$ and a surface density $N/S = 1.2\sigma_0^{-2}$.

interparticle repulsive interactions. In addition, the local mean size, $\langle\sigma(z)\rangle$, as shown in Fig. 2(c), exhibits an intriguing behavior near the wall. Typically, in the bulk, the mean size is expected to decrease as ρ increases.[9] However, near the walls, an increase in $\langle\sigma\rangle$ is observed as ρ increases, a phenomenon also noted in equilibrium configurations.[66] This behavior can be explained by the conditions faced by colloids near a hard boundary. Unlike in the bulk, where colloids are fully surrounded by other particles, being near a wall reduces the number of neighboring particles by roughly a factor of two. This reduction in surrounding particles diminishes the overall repulsive forces acting on the colloids, allowing them to expand. This effect arises from the application of ideal hard walls in our model. Here, the centers of mass of the colloids can approach the walls located at $z = 0$ and $z = L$ without encountering any repulsive interaction. However, in a more realistic scenario, the deformation of the soft particles near the wall introduces an additional distance-dependent repulsive force that should be incorporated into the model, such as the effective wall–particle repulsion observed in self-avoiding linear polymer chains in a good solvent near a hard wall.[84,93] Accounting for this additional contribution to u_{walls} would result in a reduction in the particle size when colloids are in the close vicinity of one of the walls,[66] competing with the observed trends in the current model.

Upon activation of the gravitational field $\phi_{\text{G}}(z)$ at time $t > 0$, the system is subjected to a reordering as particles migrate toward the region with a lower external field, located on the left side of the slit. This process, depicted in the dynamic sequence in Figs. 2(a) and 2(c), is not instantaneous; thus, we plot the density and mean size at various times to capture the evolution. It is interesting to remark the strong change of $\langle\sigma(z)\rangle$ during the first stages of the evolution ($0.5\tau_{\text{B}}$), compared to the evolution of $\rho(z;t)$. Given that $\alpha = 0.1$ implies that size diffusion should be significantly slower than spatial diffusion, the observed rapid change in size must be necessarily caused by Stokes-type diffusion, $D_{\text{T}} \sim 1/\sigma$: Smaller particles, having a higher diffusion coefficient, move faster toward the left, leaving behind larger particles and thus increasing the average size on the right side of the system. In addition, a decrease in density favors more expanded states for the particles.

The system keeps evolving, and we illustrate these dynamics only up to $3\tau_{\text{B}}$ because the changes become exceedingly slow thereafter. By $10\tau_{\text{B}}$, the system reaches a state indistinguishable from the equilibrium state achieved under the gravitational field. In this final equilibrium state, which is also the starting point for the deactivation process [Figs. 2(b) and 2(d)], the density ρ decays from the left wall. In an ideal, non-interacting system, this decay would be purely exponential. However, due to the existent repulsive interactions between colloids, the actual final equilibrium density profile departs from this ideal behavior. Excluding the near-wall effects previously discussed, regions with higher particle concentration correspond to smaller mean sizes, indicating compression due to increased density. Interestingly, near the right wall, where ρ is nearly zero, the mean size is maximal and very close to one, suggesting negligible interparticle interactions as the size distribution aligns with the parent distribution, $p(\sigma)$. The complete dynamics of the activation process depicted in Fig. 1 are illustrated through representative snapshots obtained from Brownian Dynamics (BD) simulations, capturing the initial, intermediate, and final states. As depicted, upon activation of

$\phi_{\text{G}}(z)$, responsive particles undergo noticeable diffusion toward the left wall. This results in compression, leading to a significant localization effect in particle size when compared to the less compressed region near the right wall.

Additional results obtained using RC-DDFT with a unimodal size distribution (i.e., with only a single peak) are presented in Sec. S1 of the supplementary material. We find that, although the results are qualitatively similar, the single-peak distribution limits the variability in particle size, except under extreme compression conditions. In contrast, a bimodal size distribution allows the particle size to switch between large and small under compression or the application of an external field, thereby emphasizing the observed changes, especially in $\langle\sigma(z;t)\rangle$. However, we demonstrate that the dynamic behavior of the bimodal parent distribution can be replicated using a broader unimodal distribution with a larger softness parameter.

Figures 2(b) and 2(d) show again $\rho(z;t)$ and $\langle\sigma(z;t)\rangle$ for the deactivation process, respectively. In this case, we find that the migration toward the new equilibrium state is not symmetrical compared to the activation process. During activation, particle movement is driven by the external gravitational force, whereas upon deactivation, particle movement is driven by the gradient of concentration, which pushes the particle from the more dense region (left) to the more dilute one (right). This asymmetry results in differing dynamics between activation and deactivation phases, with the gravitational field's application appearing to accelerate the dynamic process as it will be discussed later.

We can obtain a clearer description of the nonequilibrium dynamics by examining the position-dependent size distribution obtained via RC-DDFT, $f(\mathbf{r}, \sigma; t)$, as defined in Eq. (17). Figure 3 shows three snapshots of this distribution upon activation of the gravitational field. Initially, at $t = 0$, there is a higher concentration of large particles near the wall compared to the bulk, as previously described. Over time, $f(\mathbf{r}, \sigma; t)$ evolves at each position, increasing the proportion of large particles where the density decreases and increasing the proportion of small particles in more crowded regions. At final equilibrium, the distribution at $z = 6\sigma_0$ is almost identical to $p(\sigma)$. This is due to the very low density at that point, $\rho(6\sigma_0, \infty) \approx 0$, which implies very weak interparticle interactions and, consequently, no compression. Moving toward the other wall ($L = 0$), $f(\mathbf{r}, \sigma; t)$ transitions to a new distribution where almost all responsive colloids are in the small state.

Additional results performed with a larger surface density of colloids are shown in Sec. S2 of the supplementary material in order to exemplify even larger crowding effects.

B. Osmotic potential

Next, we turn to examine the dynamics of the RC fluid when the osmotic potential is activated and deactivated [Eq. (26)]. This external potential varies linearly with z, akin to gravitational force, but its pronounced σ^3-dependency gives rise to a markedly distinct qualitative dynamic behavior. Figures 4(a) and 4(c) illustrate the mean particle density and mean size within the planar slit during the activation process, respectively, while Figs. 4(b) and 4(d) delineate the same quantities during deactivation. We maintain $\alpha = 0.1$ and $N/S = 1.2\sigma_0^{-2}$.
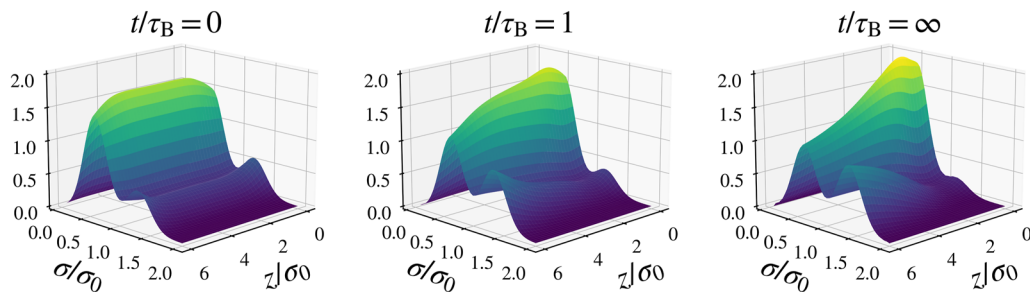
FIG. 3. Snapshots of $f(z, \sigma; t)$ at three different times obtained after activation of the gravitational field at $t > 0$ using RC-DDFT. Calculations are performed considering $\alpha = 0.1$, $N/S = 1.2\sigma_0^{-2}$, and $\tau/\sigma_0 = 0.2$.
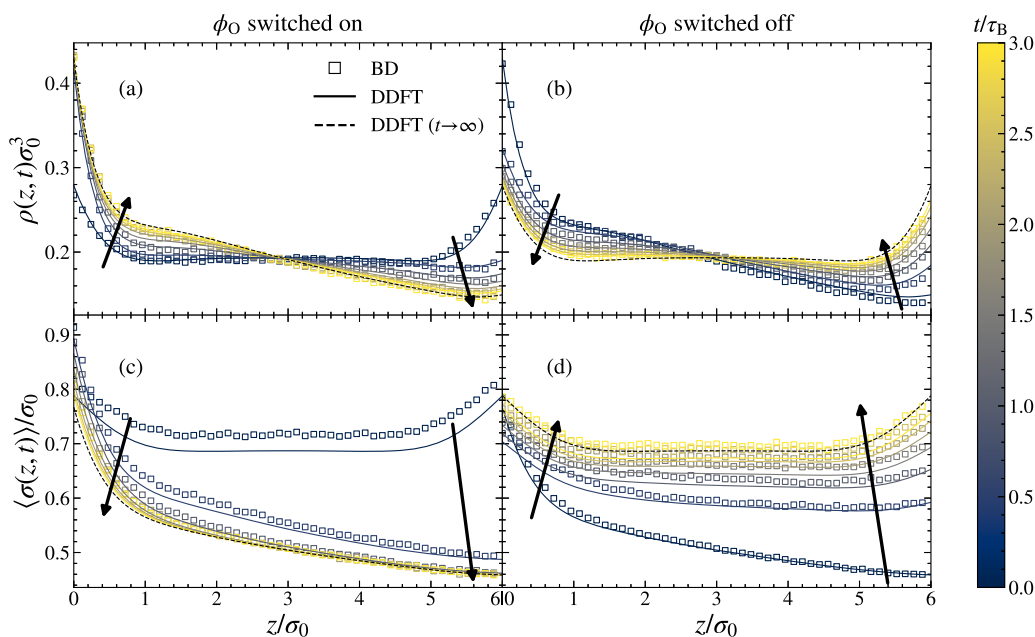

FIG. 4. Time evolution of the RCs in the osmotic field, $\phi_O(z, \sigma)$, plotted at different times ranging from $t = 0$ (dark blue) to $3\tau_B$ (yellow), with a time interval of $\Delta t = 0.5\tau_B$. The solid lines represent the theoretical predictions obtained with RC-DDFT, whereas the symbols correspond to BD simulations. The dashed lines depict the final equilibrium. Panels (a) and (c) show, respectively, the local density ($\rho(z; t)$) and the local mean size ($\langle\sigma(z; t)\rangle$) obtained when the external potential is switched on for $t > 0$. Similarly, panels (b) and (d) show the same quantities, but for the deactivation process. All calculations are performed considering $\alpha = 0.1$ and a surface density $N/S = 1.2\sigma_0^{-2}$.

Upon activation of $\phi_O(z, \sigma)$, particles tend to migrate globally toward the left, mitigating the energy contribution induced by the external potential, expressed as $\int \rho\phi_O dz d\sigma$. Analogous to gravitational effects, this results in a notable increase in particle density near the left wall over time.

However, $\langle\sigma(z; t)\rangle$ exhibits a contrasting behavior, with larger particle sizes accompanying high-density regions, as depicted in Fig. 4(c). This occurs despite the compression near the left wall. This phenomenon can be elucidated by the strong dependence of $\phi_O(z, \sigma)$ on σ: the energetic penalty for larger colloids near the right wall prompts smaller colloids to prevail in that region. In addition,

$\langle\sigma(z; t)\rangle$ experiences a rapid decline in early stages of evolution ($t < 0.5\tau_B$), not attributable to RC shrinkage, given that calculations are conducted with a deswelling diffusion 10 times smaller than spatial diffusion. This effect stems from the migration of larger colloids toward the left wall, propelled by the applied external force, $f_{ext} = -d\phi_O/dz = -A\sigma^3$.

A distinct dynamical behavior emerges upon deactivating the osmotic potential. Remarkably, convergence is achieved within $3\tau_B$ in both scenarios. However, activating the osmotic potential leads to markedly faster dynamics compared to its deactivation. This acceleration is particularly pronounced when examin-

ing the size distribution, with temporal profiles nearly coinciding after just $t \approx \tau_B$.

Furthermore, a transient behavior is observed upon activation of $\phi_O(z, \sigma)$. Indeed, after activation, there is a rapid migration of colloids toward the left wall, resulting in a significant concentration increase at very short times in this region. Concurrently, the mean particle size of colloids near the left wall initially increases, followed by a decay over longer times. This clearly indicates that particles first move to the left and then decreases their size. Conversely, deactivating $\phi_O(z, \sigma)$ yields the opposite trend, with ρ and σ increasing on the left and decreasing on the right until equilibrium is attained.

In both scenarios (activation and deactivation), the comparison between theoretical predictions from RC-DDFT and BD simulations demonstrates very good agreement.

C. Macroscopic analysis

To validate the agreement between RC-DDFT and BD beyond the local density and size profiles, we examine three interesting macroscopic, integrated quantities. These quantities not only offer insights into the global behavior of the system but also facilitate a comparison of the time scales on which dynamical processes occur. The quantities of interest are the center of mass position $\langle z \rangle$ of the suspension [Eq. (18)], the global mean particle size $\langle \sigma(t) \rangle$

[Eq. (20)], and the pressures exerted by the RC fluid on the left and right hard walls, given by $P_{\text{left}}(t)$ and $P_{\text{right}}(t)$ [Eq. (21)], respectively.

The time evolution of these quantities is illustrated in Fig. 5 for $\alpha = 0.1$ and $N/S = 1.2\sigma_0^{-2}$. Each panel presents results obtained from RC-DDFT for activated (solid lines) and deactivated (dashed lines) gravitational and osmotic external potentials, distinguished by orange and blue lines, respectively. The corresponding BD simulations are represented by squared and circled symbols. A remarkable congruence between macroscopic quantities is derived from both RC-DDFT and BD, not only in shape but also in indicative time scales (the values of $\langle \sigma(z; t) \rangle$ obtained via RC-DDFT for the gravitational cases have been rescaled here, too, by a factor of 1.05 for a clearer comparison with the simulation data).

The analysis of these curves reveals several features of the relaxation process. Primarily, it is evident that relaxation during the activation of the external field is consistently faster than during deactivation. We attribute this behavior to the supplementary driving force induced by the activated external potential, intensifying the motion of confined colloids. Conversely, during the deactivation process, this external force is absent, so colloids rely solely on diffusion for movement, thereby leading to a slower evolution toward equilibrium.
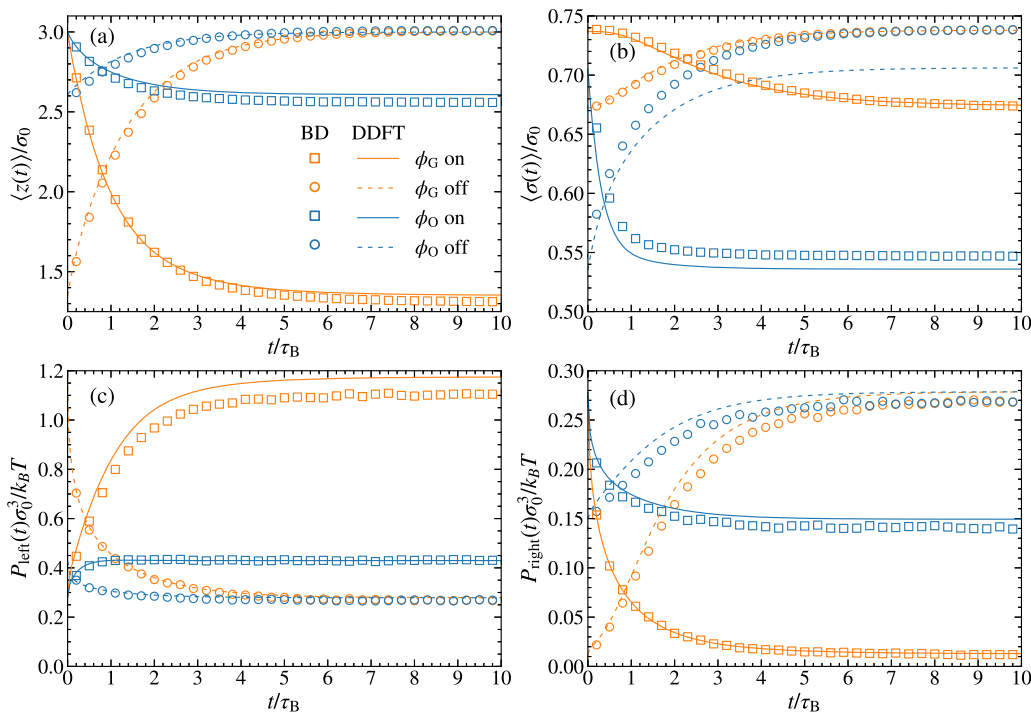

FIG. 5. Time evolution of (a) the center of mass position ($\langle z(t) \rangle$), (b) the mean particle size of the system ($\langle \sigma(t) \rangle$), with gravitational RC-DDFT data multiplied by 1.05 for a better comparison with simulations, and (c) the pressure applied by the fluid on the left wall ($P_{\text{left}}(t)$) and (d) on the right wall ($P_{\text{right}}(t)$), obtained for the activation (solid lines) and deactivation (dashed lines) processes. The orange and blue colors represent the results for the gravitational and osmotic potentials, respectively. The lines denote the RC-DDFT predictions, whereas the symbols denote the BD simulations. In all cases, $\alpha = 0.1$ and surface density $N/S = 1.2\sigma_0^{-2}$.

TABLE I. Relaxation times obtained by fitting Eq. (27) to mean size, $\langle\sigma(t)\rangle$, and mean position, $\langle z(t)\rangle$, predicted by RC-DDFT during the activation (on) and deactivation (off) of the external potentials, $\phi_G(z)$ and $\phi_O(z,\sigma)$. The corresponding times for BD simulations are shown within the parentheses.

	τ	ϕ_G (on)	ϕ_G (off)	ϕ_O (on)	ϕ_O (off)
$\langle z\rangle$	τ_1	0.90 (0.91)	1.38 (1.47)	0.24 (0.25)	1.33 (1.46)
	τ_2	1.97 (1.95)	1.38 (1.47)	1.23 (1.23)	1.33 (1.46)
$\langle\sigma\rangle$	τ_1	1.08 (1.15)	0.61 (0.72)	0.30 (0.31)	0.28 (0.27)
	τ_2	1.69 (1.83)	1.50 (1.55)	1.20 (1.42)	1.48 (1.61)

With our system's inherent two degrees of freedom, we employ a double exponential function to fit these macroscopic quantities, facilitating the extraction of time scales,

$$\psi(t) = A_1 e^{-t/\tau_1} + A_2 e^{-t/\tau_2} + c, \qquad (27)$$

being $\psi(t) = \{\langle z(t)\rangle, \langle\sigma(t)\rangle\}$. The relaxation times, τ_1 and τ_2, obtained from these fits, are summarized in Table I, presenting a comparison of the time scales predicted by RC-DDFT and observed through BD (between parentheses) under the scenarios studied.

In every scenario, we observe two distinct time scales that are similar within each potential and across both RC-DDFT and BD analyses. This similarity suggests that the complex dynamics of the system are influenced by the interaction between translational and size diffusion processes. The differences in the shapes of macroscopic quantities for various potentials, as shown in Fig. 5, likely

arise from the differing impacts of these time scales. The close match between macroscopic quantities obtained from BD simulations and those predicted by RC-DDFT highlights the effectiveness of the RC-DDFT extension in accurately capturing the dynamics of the system. This concordance further supports the use of RC-DDFT for additional studies.

As summarized in Table I, the relaxation time for $\langle z(t)\rangle$ when ϕ_O is switched on $(0.24\tau_B)$ and off $(1.33\tau_B)$ or the relaxation time for $\langle\sigma(t)\rangle$ when ϕ_G is switched on $(1.08\tau_B)$ and off $(0.61\tau_B)$ is a clear signature of irreversible relaxation pathway. In addition, the difference in relaxation time for $\langle z(t)\rangle$ when switching on ϕ_O and ϕ_G reveals that the nature of the perturbation has an important effect on the relaxation process (see Fig. 5).

D. Competition of time scales: The α-study

Having evaluated the effects of the activation and deactivation processes of the external field, we now focus on the assessment of the influence of the time scale ratio, $\alpha = D_\sigma/D_0$, on the non-equilibrium relaxation dynamics of our confined system of soft RCs. As mentioned earlier, α modulates the interplay between size diffusion and translational diffusion. For such a study, we select the osmotic external potential and consider only the activation process. Figure 6 shows the time evolution of $\rho(z;t)$ and $\langle\sigma(z;t)\rangle$ for $\alpha = 1$ [panels (a) and (c)] and $\alpha = 0.01$ [panels (b) and (d)], representing two limiting dynamic conditions for which the σ-diffusion is very fast and very slow compared to the translational diffusion. Please note that even though for $\alpha = 1$ spatial and swelling diffusion times are on comparable scales, the colloids need to travel a distance of
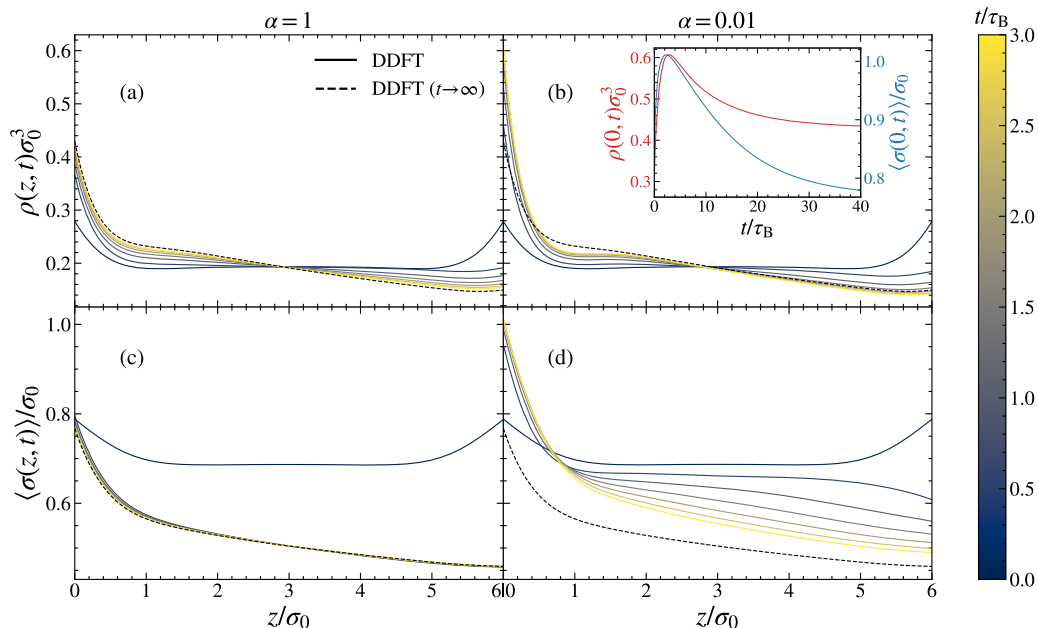

FIG. 6. RC-DDFT results for the time evolution of the system's structure for the osmotic field, ϕ_O, being switched on at time $t = 0$ for various values of the time scale parameter α. The dashed lines depict the final equilibrium. (a), (b) Local density, $\rho(z)$, and (c), (d) local mean size, $\langle\sigma(z)\rangle$, at different times ranging from 0 τ_B (blue) to 3 τ_B (yellow) with a time interval of 0.5 τ_B. The surface density is $N/S = 1.2\sigma_0^{-2}$. The inset in (b) shows the time evolution of the density ρ and the mean size $\langle\sigma\rangle$ on the left wall.

the order of $6\sigma_0$ (the distance between both walls) to reach spatial equilibrium, whereas particle sizes only need to vary by about $0.74\sigma_0$ (the separation between the peaks of $p(\sigma)$) to achieve equilibrium, which is almost 10 times smaller. Therefore, $\alpha \approx 0.1$ represents the appropriate value that separates "slow" vs "fast" size response in our system when compared to translation. Note that the final equilibrium state (for $t \to \infty$) is depicted as a black dashed line in each plot. The particle surface concentration is fixed in all cases to $N/S = 1.2\sigma_0^{-2}$. Considering the close alignment between RC-DDFT and BD observed in Secs. IV A–IV C, we only depict the results obtained with RC-DDFT.

For $\alpha = 1$, the particle size rapidly adjusts to the new environmental conditions during the initial relaxation stage, and the system approaches full structural equilibrium within $3\tau_B$. Decreasing α to 0.01 results in a slower response of particle size to the activation of the external potential. As observed, the time evolution in this case is so slow that the system does not reach the final equilibrium state within the plotted $t \le 3\tau_B$. Notably, in this small-α regime, our findings reveal the presence of a transient dynamic state in the early dynamics: initially, particles accumulate on the left wall for $t < 3\tau_B$, followed by a subsequent decrease in concentration toward the final equilibrium state for $t > 3\tau_B$. This dynamic non-monotonic behavior is clearly depicted in the inset of Fig. 6(b), illustrating the time dependence of the particle density in contact with the left hard wall, $\rho(z = 0; t)$, which exhibits a maximum at $t \approx 3\tau_B$. A similar trend is observed for the mean size of colloids in contact with the left wall ($\langle\sigma(z = 0; t)\rangle$), initially increasing with time before eventually decreasing again [see again the inset of Fig. 6(b)]. In the inset, we can also clearly see the relaxation to equilibrium for long times.

It is important to highlight that this transient dynamic state observed at intermediate times arises directly from the disparity in time scales between translation and swelling, evident for $\alpha = 0.01$ and absent for $\alpha = 1$. Initially, colloids diffuse toward the left under the external field without altering their size, which evolves 100 times slower. The observed increase in $\langle\sigma(z = 0; t)\rangle$ is primarily attributed to the selective motion of larger colloids driven by the applied external force $f_{ext} = -d\phi_0/dz = -A\sigma^3$. Over longer time scales, compression effects lead to a gradual (slower) reduction in particle size, consequently inducing a decrease in $\rho(z = 0; t)$ until the new equilibrium state is attained. In essence, this observation signifies a transition from translationally driven to size-driven relaxation dynamics as α decreases from 1 to 0.01, a characteristic exclusive to responsive colloids.

This rich interplay between structural and size relaxation is further illustrated in Figs. 7(a) and 7(b), which explore, respectively, the impact of α on the center of mass position ($\langle z(t)\rangle$) and on the mean particle size ($\langle\sigma(t)\rangle$) across a wide range of α values from 0.01 to 2. In cases where $\alpha < 0.04$, a non-monotonic curve with a pronounced minimum appears in $\langle z(t)\rangle$, signifying that responsive colloids initially migrate toward the left wall due to the applied external force before subsequently reversing direction due to gradual size reduction. Conversely, for $\alpha > 0.25$, the opposing trend is found: the particle size undergoes a rapid reduction attributed to the compression induced by the osmotic field during the initial stages of evolution, yet the colloids have not traversed the necessary distance to achieve structural relaxation. For longer times, the progressive redistribution of colloids toward the left wall through spatial diffu-
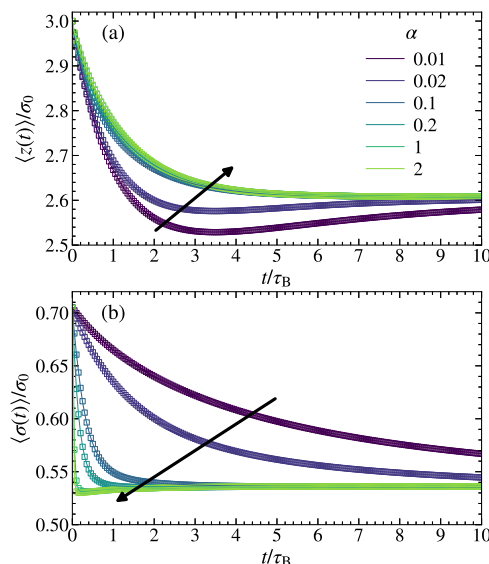

FIG. 7. Time evolution of (a) the center of mass position ($\langle z(t)\rangle$) and (b) the mean size of the colloids ($\langle\sigma(t)\rangle$) predicted by RC-DDFT (symbols) during the activation of the osmotic external potential, obtained for different values of α from 0.01 to 2. The solid lines are the result of the fitting of the data using Eq. (27). In all cases, $N/S = 1.2\sigma_0^{-2}$.

sion allows $\langle\sigma(t)\rangle$ to exhibit a slight increase, driven by the swelling of colloids near $z = 0$.

This transient behavior observed for dissimilar values of D_T and D_σ becomes evident in Fig. 8, where $\langle z(t)\rangle$ is plotted against $\langle\sigma(t)\rangle$ for different values of α, from 0.01 to 3. Indeed, for $\alpha = 0.01$, we find that $\langle z(t)\rangle$ shows a non-monotonic behavior induced by the slow σ-response, leading to a minimum in the curve. Conversely, for $\alpha = 3$, the curve depicts a shoulder on the left, indicating the non-monotonicity of the center of mass location caused by the slow translational diffusion. These phenomena controlled by α demonstrate the dynamic competition between translational and size diffusion. At very low or high α values, the dynamics of mean size and position appear closely coupled, depicting a scenario where one aspect of the system's behavior must "wait" for the other to stabilize.

The fitting of the center of mass position and mean particle size after activation of $\phi_0(z, \sigma)$ according to the double exponential function given by Eq. (27) yields relaxation times and prefactors as a function of α, as shown in Fig. 9. This analysis confirms the presence of two distinct time scales, corresponding to translational and size diffusion processes. We identify τ_1 as the translational relaxation time and τ_2 as the size relaxation time, with A_1 and A_2 denoting the corresponding prefactors for translational and size relaxation, respectively. Figure 9(a) shows the behavior of τ_1 and τ_2 obtained from fitting $\langle z(t)\rangle$. As observed, $\tau_1 < \tau_2$ for small α, as expected for this α-regime. Conversely, for large enough α, we find that $\tau_1 > \tau_2$. In this case, size relaxation is faster, and the ultimate relaxation of $\langle z(t)\rangle$ is governed by the translation of the colloids. The crossover between these two dynamic regimes occurs at the critical value $\alpha_c \approx 0.044$, where τ_2 shows a discontinuity. The regime
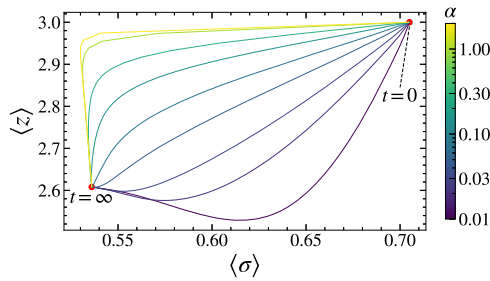
FIG. 8. Transition pathways: center of mass location $\langle z \rangle$ vs the mean particle size $\langle \sigma \rangle$ of the system during the relaxation process after activation of the osmotic external potential, plotted for different values of α. The red point on the right-top represents the initial equilibrium state ($t = 0$), whereas the one located on the left-bottom corresponds to the emerging final equilibrium state ($t \to \infty$). Results are obtained using RC-DDFT with $N/S = 1.2\sigma_0^{-2}$.

$\alpha > \alpha_c$ corresponds to normal relaxation, where translational relaxation predominates as the main mechanism controlling the location of the system's center of mass, and the sign of both prefactors A_1 and A_2 is positive, as depicted in Fig. 9(b). However, the regime $\alpha < \alpha_c$ represents a situation where translational relaxation occurs following a change in size, causing $\langle z(t) \rangle$ to be driven by size adjustments. This regime is clearly identified because one of the prefactors, in this case A_2, takes negative values, leading to the previously discussed non-monotonic dynamic behavior. The exact crossover between times occurs when $A_2 = 0$, indicated by a red vertical line in Figs. 9(a) and 9(b)

Examining the behavior of τ_1 and τ_2 obtained by fitting $\langle \sigma(t) \rangle$, as depicted in Fig. 9(c), we observe a similar dynamic pattern: relaxation toward equilibrium is dominated by size adjustments ($\tau_1 < \tau_2$) when α is small and by translational diffusion ($\tau_1 > \tau_2$) for larger values of α. In this second regime, colloids first adjust their size to the initial structure and later, as the system restructures due to the external field, they readjust their size. As seen in Fig. 9(d), this second regime is characterized by negative values of A_1, leading to transient states, where colloids initially shrink and then swell due to their spatial reallocation in a second stage. The crossover between both regimes occurs at $\alpha_c \approx 0.3$. The difference between the α_c values reported for $\langle z(t) \rangle$ and $\langle \sigma(t) \rangle$ arises from the greater distance that responsive colloids need to travel to reach equilibrium compared to the range of size variation.

V. CONCLUDING REMARKS

In this work, we have developed and combined a dynamic density-functional theory (RC-DDFT) framework and Brownian dynamics (BD) simulations to investigate the full time-dependent non-equilibrium relaxation dynamics of confined systems of soft responsive colloids (RCs) after the activation/deactivation of external potentials. In contrast to conventional models of soft colloids, in our model, the size dynamics of the colloids is explicitly resolved and the influence of its relaxation behavior and time scale on the full system's dynamics could be explored for the first time. The results showed a complex interplay between the translational diffusion and the particle swelling/shrinking dynamics, leading to interesting non-equilibrium structuring as well as non-monotonic transient behaviors when the typical spatial and size relaxation time scales are
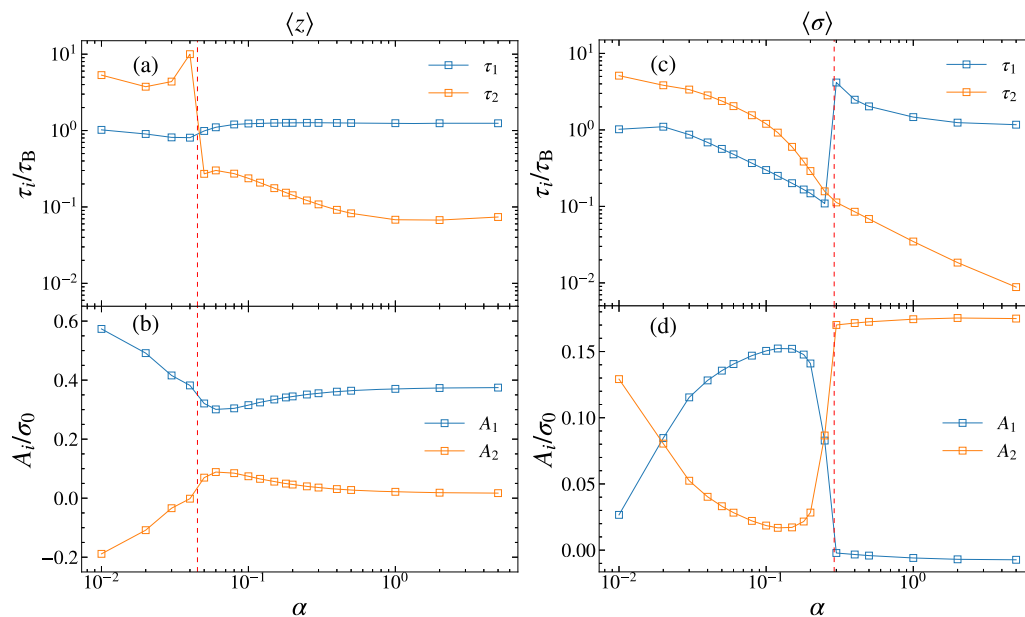

FIG. 9. Relaxation times, τ_i, and prefactors, A_i, as a function of α. They are obtained by fitting $\langle z(t) \rangle$ [panels (a) and (b)] and $\langle \sigma(t) \rangle$ [panels (c) and (d)] predicted by RC-DDFT to Eq. (27), during the activation process of the osmotic external potential, for $N/S = 1.2\sigma_0^{-2}$. The vertical lines show the crossover between τ_1 and τ_2, which happens if one of the prefactors, A_1 or A_2, is zero. The data correspond to the structural time evolution shown in Fig. 7.

very different. We also demonstrated that the modification of intrinsic time scales of the system leads to tunable macroscopic relaxation times and pathways in systems with many relaxing degrees of freedom. The excellent agreement between DDFT and BD showed that DDFT can also be faithfully used to study the nonequilibrium behavior of soft, weakly correlated colloids with additional internal degrees of freedom, if the systems are not too slaved by dissipative mechanisms.[92] Hence, our study constitutes a big step forward for the modeling and description of the full nonequilibrium structuring of soft complex fluids.

In the future, it would be interesting to extend the RC-DDFT method to responsive (intrinsically polydisperse) systems of stiffer systems, e.g., microgels modeled by Hertzian potentials.[7,39] For these systems, we expect to find marked oscillations of the density profiles that will become strongly affected by particle stiffness. In addition, the dynamical properties can lead to the formation of interesting transient, e.g., highly structured while full nonequilibrium regions that finally relax when the colloids adapt their size to the new environmental conditions. These transients may have interesting new properties. Finally, one could also envision to add more internal degrees of freedom to the colloids with a more complex hierarchy of time scales, or even add internal chemical activity to the colloids, e.g., as used in catalytically active nanoreactors where the bistable size response is crucial for complex self-dynamics.[94]

SUPPLEMENTARY MATERIAL

Additional results obtained using RC-DDFT with a unimodal parent size distribution are presented in Sec. S1 of the supplementary material. The parent size distribution, $p(\sigma)$, for bimodal and unimodal distributions with different softness parameters, $\tau/\sigma_0 = 0.2$ and 0.3, is plotted in Fig S1.1 of the supplementary material. The time evolution of $\rho(z;t)$ and $\langle\sigma(z;t)\rangle$ is plotted in Fig S1.2 of the supplementary material, while the nonequilibrium relaxation of the center of mass position is plotted in Fig. S1.3 of the supplementary material for the considered unimodal parent size distribution. Furthermore, additional results performed with a larger surface density of colloids and a bimodal parent size distribution are presented in Sec. S2 of the supplementary material in order to exemplify even larger crowding effects. RC-DDFT results for the time evolution of the system's structure for the osmotic field, ϕ_O, being switched on at time $t = 0$ for various values of the time scale parameter α are plotted in Fig. S2.1 of the supplementary material, while the time evolution of the center of mass position $\langle z(t)\rangle$ and the mean size of the colloids $\langle\sigma(z;t)\rangle$ is plotted in Fig. S2.2 of the supplementary material.

ACKNOWLEDGMENTS

AUTHOR DECLARATIONS

Conflict of Interest

The authors have no conflicts to disclose.

Author Contributions

José López-Molina: Conceptualization (equal); Data curation (equal); Investigation (equal); Methodology (equal); Software (equal); Validation (equal); Writing – original draft (equal); Writing – review & editing (equal). **Sebastien Groh**: Conceptualization (equal); Data curation (equal); Investigation (equal); Methodology (equal); Software (equal); Validation (equal); Writing – original draft (equal); Writing – review & editing (equal). **Joachim Dzubiella**: Conceptualization (equal); Data curation (equal); Investigation (equal); Methodology (equal); Software (equal); Supervision (equal); Validation (equal); Writing – original draft (equal); Writing – review & editing (equal). **Arturo Moncho-Jordá**: Conceptualization (equal); Data curation (equal); Investigation (equal); Methodology (equal); Software (equal); Supervision (equal); Validation (equal); Writing – original draft (equal); Writing – review & editing (equal).

DATA AVAILABILITY

The data that support the findings of this study are available from the corresponding author upon reasonable request.

REFERENCES

[1] M. A. C. Stuart, W. T. S. Huck, J. Genzer, M. Müller, C. Ober, M. Stamm, G. B. Sukhorukov, I. Szleifer, V. V. Tsukruk, M. Urban, F. Winnik, S. Zauscher, I. Luzinov, and S. Minko, "Emerging applications of stimuli-responsive polymer materials," Nat. Mater. **9**, 101 (2010).

[2] J. N. Onuchic, Z. Luthey-Schulten, and P. G. Wolynes, "Theory of protein folding: The energy landscape perspective," Annu. Rev. Phys. Chem. **48**, 545–600 (1997).

[3] C. Wu and X. Wang, "Globule-to-coil transition of a single homopolymer chain in solution," Phys. Rev. Lett. **80**, 4092–4094 (1998).

[4] S. S. Cho, Y. Levy, and P. G. Wolynes, "*P* versus *Q*: Structural reaction coordinates capture protein folding on smooth landscapes," Proc. Natl. Acad. Sci. U.S.A. **103**, 586–591 (2006).

[5] U. B. Choi, J. J. McCann, K. R. Weninger, and M. E. Bowen, "Beyond the random coil: Stochastic conformational switching in intrinsically disordered proteins," Structure **19**, 566–576 (2011).

[6] A. R. Denton and M. Schmidt, "Colloid-induced polymer compression," J. Phys.: Condens. Matter **14**, 12051–12062 (2002).

[7] M. Urich and A. R. Denton, "Swelling, structure, and phase stability of compressible microgels," Soft Matter **12**, 9086–9094 (2016).

[8] J. Brijitta and P. Schurtenberger, "Responsive hydrogel colloids: Structure, interactions, phase behavior, and equilibrium and nonequilibrium transitions of microgel dispersions," Curr. Opin. Colloid Interface Sci. **40**, 87–103 (2019).

[9] U. Baul and J. Dzubiella, "Structure and dynamics of responsive colloids with dynamical polydispersity," J. Phys.: Condens. Matter **33**, 174002 (2021).

[10] U. Baul, N. Göth, M. Bley, and J. Dzubiella, "Modulating internal transition kinetics of responsive macromolecules by collective crowding," J. Chem. Phys. **155**, 244902 (2021).

[11] Y.-C. Lin, B. Rotenberg, and J. Dzubiella, "Structure and position-dependent properties of inhomogeneous suspensions of responsive colloids," Phys. Rev. E **102**, 042602 (2020).

[12] H. Meng and G. Li, "Reversible switching transitions of stimuli-responsive shape changing polymers," J. Mater. Chem. A **1**, 7838–7865 (2013).

[13] J. Lee, K. H. Ku, C. H. Park, Y. J. Lee, H. Yun, and B. J. Kim, "Shape and color switchable block copolymer particles by temperature and pH dual responses," ACS Nano **13**, 4230–4237 (2019).

[14] W. K. Lim and A. R. Denton, "Polymer crowding and shape distributions in polymer-nanoparticle mixtures," J. Chem. Phys. **141**, 114909 (2014).

[15] W. K. Lim and A. R. Denton, "Depletion-induced forces and crowding in polymer-nanoparticle mixtures: Role of polymer shape fluctuations and penetrability," J. Chem. Phys. **144**, 024904 (2016).

[16] W. K. Lim and A. R. Denton, "Influence of polymer shape on depletion potentials and crowding in colloid–polymer mixtures," Soft Matter **12**, 2247–2252 (2016).

[17] J. Harrer, M. Rey, S. Ciarella, H. Löwen, L. M. C. Janssen, and N. Vogel, "Stimuli-responsive behavior of pnipam microgels under interfacial confinement," Langmuir **35**, 10512–10521 (2019).

[18] G. Del Monte and E. Zaccarelli, "Numerical study of neutral and charged microgel suspensions: From single-particle to collective behavior," arXiv:2404.04032 (2024).

[19] R. Elancheliyan, G. Del Monte, E. Chauveau, S. Sennato, E. Zaccarelli, and D. Truzzolillo, "Role of charge content in the two-step deswelling of poly(N-isopropylacrylamide)-Based microgels," Macromolecules **55**, 7526–7539 (2022).

[20] T. J. Weyer and A. R. Denton, "Concentration-dependent swelling and structure of ionic microgels: Simulation and theory of a coarse-grained model," Soft Matter **14**, 4530–4540 (2018).

[21] J. Cao and B. J. Berne, "Theory and simulation of polar and nonpolar polarizable fluids," J. Chem. Phys. **99**, 6998–7011 (1993).

[22] D. F. Calef and P. G. Wolynes, "Smoluchowski–Vlasov theory of charge solvation dynamics," J. Chem. Phys. **78**, 4145–4153 (1983).

[23] A. Chandra and B. Bagchi, "Collective orientational relaxation in a dense liquid of ellipsoidal molecules," Physica A **169**, 246–262 (1990).

[24] A. Chandra and B. Bagchi, "The role of translational diffusion in the polarization relaxation in dense polar liquids," Chem. Phys. Lett. **151**, 47–53 (1988).

[25] M. Motornov, R. Sheparovych, R. Lupitskyy, E. MacWilliams, and S. Minko, "Responsive colloidal systems: Reversible aggregation and fabrication of superhydrophobic surfaces," J. Colloid Interface Sci. **310**, 481–488 (2007).

[26] M. Motornov, H. Royter, R. Lupitskyy, Y. Roiter, and S. Minko, "Stimuli-responsive hydrogel hollow capsules by material efficient and robust cross-linking-precipitation synthesis revisited," Langmuir **27**, 15305–15311 (2011).

[27] K. Kalaitzidou and A. J. Crosby, "Adaptive polymer particles," Appl. Phys. Lett. **93**, 041910 (2008).

[28] M. S. Cheung, D. Klimov, and D. Thirumalai, "Molecular crowding enhances native state stability and refolding rates of globular proteins," Proc. Natl. Acad. Sci. U.S.A. **102**, 4753–4758 (2005).

[29] H.-X. Zhou, G. Rivas, and A. P. Minton, "Macromolecular crowding and confinement: Biochemical, biophysical, and potential physiological consequences," Annu. Rev. Biophys. **37**, 375–397 (2008).

[30] J. Hong and L. M. Gierasch, "Macromolecular crowding remodels the energy landscape of a protein by favoring a more compact unfolded state," J. Am. Chem. Soc. **132**, 10445–10452 (2010).

[31] N. F. Dupuis, E. D. Holmstrom, and D. J. Nesbitt, "Molecular-crowding effects on single-molecule rna folding/unfolding thermodynamics and kinetics," Proc. Natl. Acad. Sci. U.S.A. **111**, 8464–8469 (2014).

[32] J. Shin, A. G. Cherstvy, and R. Metzler, "Kinetics of polymer looping with macromolecular crowding: Effects of volume fraction and crowder size," Soft Matter **11**, 472–488 (2015).

[33] S. Huang, K. Gawlitza, R. von Klitzing, L. Gilson, J. Nowak, S. Odenbach, W. Steffen, and G. K. Auernhammer, "Microgels at the water/oil interface: In situ observation of structural aging and two-dimensional magnetic bead microrheology," Langmuir **32**, 712–722 (2016).

[34] V. Garbin, I. Jenkins, T. Sinno, J. C. Crocker, and K. J. Stebe, "Interactions and stress relaxation in monolayers of soft nanoparticles at fluid-fluid interfaces," Phys. Rev. Lett. **114**, 108301 (2015).

[35] T. Vettorel, G. Besold, and K. Kremer, "Fluctuating soft-sphere approach to coarse-graining of polymer models," Soft Matter **6**, 2282–2292 (2010).

[36] R. G. Winkler, D. A. Fedosov, and G. Gompper, "Dynamical and rheological properties of soft colloid suspensions," Curr. Opin. Colloid Interface Sci. **19**, 594–610 (2014).

[37] A. Moncho-Jordá and J. Dzubiella, "Swelling of ionic microgel particles in the presence of excluded-volume interactions: A density functional approach," Phys. Chem. Chem. Phys. **18**, 5372–5385 (2016).

[38] M. Karg, A. Pich, T. Hellweg, T. Hoare, L. A. Lyon, J. J. Crassous, D. Suzuki, R. A. Gumerov, S. Schneider, I. I. Potemkin, and W. Richtering, "Nanogels and microgels: From model colloids to applications, recent developments, and future trends," Langmuir **35**, 6231–6255 (2019).

[39] L. Rovigatti, N. Gnan, A. Ninarello, and E. Zaccarelli, "Connecting elasticity and effective interactions of neutral microgels: The validity of the Hertzian model," Macromolecules **52**, 4895–4906 (2019).

[40] A. Scotti, S. Bochenek, M. Brugnoni, M. A. Fernandez-Rodriguez, M. F. Schulte, J. E. Houston, A. P. H. Gelissen, I. I. Potemkin, L. Isa, and W. Richtering, "Exploring the colloid-to-polymer transition for ultra-low crosslinked microgels from three to two dimensions," Nat. Commun. **10**, 1418 (2019).

[41] A. Scotti, A. R. Denton, M. Brugnoni, J. E. Houston, R. Schweins, I. I. Potemkin, and W. Richtering, "Deswelling of microgels in crowded suspensions depends on cross-link density and architecture," Macromolecules **52**, 3995–4007 (2019).

[42] A. Scotti, "Characterization of the volume fraction of soft deformable microgels by means of small-angle neutron scattering with contrast variation," Soft Matter **17**, 5548–5559 (2021).

[43] M. Murray and M. Snowden, "The preparation, characterisation and applications of colloidal microgels," Adv. Colloid Interface Sci. **54**, 73–91 (1995).

[44] B. R. Saunders and B. Vincent, "Microgel particles as model colloids: Theory, properties and applications," Adv. Colloid Interface Sci. **80**, 1–25 (1999).

[45] A. Fernandez-Nieves, H. Wyss, J. Mattsson, and D. A. Weitz, *Microgel Suspensions: Fundamentals and Applications* (John Wiley & Sons, 2011).

[46] Y. Zhou, H. Tang, and P. Wu, "Volume phase transition mechanism of poly[oligo(ethylene glycol)methacrylate] based thermo-responsive microgels with poly(ionic liquid) cross-linkers," Phys. Chem. Chem. Phys. **17**, 25525–25535 (2015).

[47] S. Bochenek, F. Camerin, E. Zaccarelli, A. Maestro, M. M. Schmidt, W. Richtering, and A. Scotti, "In-situ study of the impact of temperature and architecture on the interfacial structure of microgels," Nat. Commun. **13**, 3744 (2022).

[48] S. V. Nikolov, A. Fernandez-Nieves, and A. Alexeev, "Behavior and mechanics of dense microgel suspensions," Proc. Natl. Acad. Sci. U.S.A. **117**, 27096–27103 (2020).

[49] N. Gnan and E. Zaccarelli, "The microscopic role of deformation in the dynamics of soft colloids," Nat. Phys. **15**, 683–688 (2019).

[50] R. Roa, W. K. Kim, M. Kanduč, J. Dzubiella, and S. Angioletti-Uberti, "Catalyzed bimolecular reactions in responsive nanoreactors," ACS Catal. **7**, 5604–5611 (2017).

[51] R. Roa, S. Angioletti-Uberti, Y. Lu, J. Dzubiella, F. Piazza, and M. Ballauff, "Catalysis by metallic nanoparticles in solution: Thermosensitive microgels as nanoreactors," Z. Phys. Chem. **232**, 773–803 (2018).

[52] M. Kanduč, W. K. Kim, R. Roa, and J. Dzubiella, "Modeling of stimuli-responsive nanoreactors: Rational rate control towards the design of colloidal enzymes," Mol. Syst. Des. Eng. **5**, 602–619 (2020).

[53] M. Hamidi, A. Azadi, and P. Rafiei, "Hydrogel nanoparticles in drug delivery," Adv. Drug Delivery Rev. **60**, 1638–1649 (2008), 2008 Editors' Collection.

25 September 2024 08:07:06

[54]B. R. Saunders, N. Laajam, E. Daly, S. Teow, X. Hu, and R. Stepto, "Microgels: From responsive polymer colloids to biomaterials," Adv. Colloid Interface Sci. **147-148**, 251–262 (2009).

[55]S. V. Vinogradov, "Nanogels in the race for drug delivery," Nanomedicine **5**, 165–168 (2010).

[56]A. Moncho-Jordá, A. Germán-Bellod, S. Angioletti-Uberti, I. Adroher-Benítez, and J. Dzubiella, "Nonequilibrium uptake kinetics of molecular cargo into hollow hydrogels tuned by electrosteric interactions," ACS Nano **13**, 1603–1616 (2019).

[57]A. Moncho-Jordá, A. B. Jódar-Reyes, M. Kanduč, A. Germán-Bellod, J. M. López-Romero, R. Contreras-Cáceres, F. Sarabia, M. García-Castro, H. A. Pérez-Ramírez, and G. Odriozola, "Scaling laws in the diffusive release of neutral cargo from hollow hydrogel nanoparticles: Paclitaxel-loaded poly(4-vinylpyridine)," ACS Nano **14**, 15227–15240 (2020).

[58]R. Evans, "The nature of the liquid-vapour interface and other topics in the statistical mechanics of non-uniform, classical fluids," Adv. Phys. **28**, 143–200 (1979).

[59]R. Evans, in *Fundamentals in Inhomogeneous Fluids*, *Chapter Density Functionals in the Theory of Nonuniform Fluids*, edited by D. Henderson (Marcel Derrer, Inc., 1992), pp. 85–176.

[60]M. Schmidt, H. Löwen, J. M. Brader, and R. Evans, "Density functional theory for a model colloid–polymer mixture: Bulk fluid phases," J. Phys.: Condens. Matter **14**, 9353 (2002).

[61]J.-P. Hansen and I. McDonald, *Theory of Simple Liquids*, 4th ed. (Academic Press, 2013).

[62]R. Evans, M. Oettel, R. Roth, and G. Kahl, "New developments in classical density functional theory," J. Phys.: Condens. Matter **28**, 240401 (2016).

[63]I. Pagonabarraga, M. E. Cates, and G. J. Ackland, "Local size segregation in polydisperse hard sphere fluids," Phys. Rev. Lett. **84**, 911–914 (2000).

[64]M. Buzzacchi, I. Pagonabarraga, and N. B. Wilding, "Polydisperse hard spheres at a hard wall," J. Chem. Phys. **121**, 11362–11373 (2004).

[65]I. Pagonabarraga and M. Cates, "A practical density functional for polydisperse polymers," Europhys. Lett. **55**, 348 (2001).

[66]A. Moncho-Jordá, S. Groh, and J. Dzubiella, "External field-driven property localization in liquids of responsive macromolecules," J. Chem. Phys. **160**, 024904 (2024).

[67]A. Moncho-Jordá, N. Göth, and J. Dzubiella, "Liquid structure of bistable responsive macromolecules using mean-field density-functional theory," Soft Matter **19**, 2832–2846 (2023).

[68]M. te Vrugt, H. Löwen, and R. Wittkowski, "Classical dynamical density functional theory: From fundamentals to applications," Adv. Phys. **69**, 121–247 (2020).

[69]U. M. B. Marconi and P. Tarazona, "Dynamic density functional theory of fluids," J. Chem. Phys. **110**, 8032–8044 (1999).

[70]A. J. Archer and R. Evans, "Dynamical density functional theory and its application to spinodal decomposition," J. Chem. Phys. **121**, 4246–4254 (2004).

[71]C. P. Royall, J. Dzubiella, M. Schmidt, and A. van Blaaderen, "Nonequilibrium sedimentation of colloids on the particle scale," Phys. Rev. Lett. **98**, 188304 (2007).

[72]M. te Vrugt, J. Bickmann, and R. Wittkowski, "Effects of social distancing and isolation on epidemic spreading modeled via dynamical density functional theory," Nat. Commun. **11**, 5576 (2020).

[73]A. Moncho-Jordá and J. Dzubiella, "Controlling the microstructure and phase behavior of confined soft colloids by active interaction switching," Phys. Rev. Lett. **125**, 078001 (2020).

[74]M. Bley, J. Dzubiella, and A. Moncho-Jordá, "Active binary switching of soft colloids: Stability and structural properties," Soft Matter **17**, 7682–7696 (2021).

[75]M. Bley, P. I. Hurtado, J. Dzubiella, and A. Moncho-Jordá, "Active interaction switching controls the dynamic heterogeneity of soft colloidal dispersions," Soft Matter **18**, 397–411 (2022).

[76]E. Sato Matsuo and T. Tanaka, "Kinetics of discontinuous volume-phase transition of gels," J. Chem. Phys. **89**, 1695–1703 (1988).

[77]A. Suzuki and H. Suzuki, "Hysteretic behavior and irreversibility of polymer gels by ph change," J. Chem. Phys. **103**, 4706–4710 (1995).

[78]K. W. Plaxco, K. T. Simons, I. Ruczinski, and D. Baker, "Topology, stability, sequence, and length: Defining the determinants of two-state protein folding kinetics," Biochemistry **39**, 11177–11183 (2000).

[79]H. K. Murnen, A. R. Khokhlov, P. G. Khalatur, R. A. Segalman, and R. N. Zuckermann, "Impact of hydrophobic sequence patterning on the coil-to-globule transition of protein-like polymers," Macromolecules **45**, 5229–5236 (2012).

[80]X. Zeng, K. M. Ruff, and R. V. Pappu, "Competing interactions give rise to two-state behavior and switch-like transitions in charge-rich intrinsically disordered proteins," Proc. Natl. Acad. Sci. U. S. A. **119**, e2200559119 (2022).

[81]S. Dhiman, A. Jain, and S. J. George, "Transient helicity: Fuel-driven temporal control over conformational switching in a supramolecular polymer," Angew. Chem., Int. Ed. **56**, 1329–1333 (2017).

[82]H. Kang, P. A. Pincus, C. Hyeon, and D. Thirumalai, "Effects of macromolecular crowding on the collapse of biopolymers," Phys. Rev. Lett. **114**, 068303 (2015).

[83]C. N. Likos, "Effective interactions in soft condensed matter physics," Phys. Rep. **348**, 267–439 (2001).

[84]P. G. Bolhuis, A. A. Louis, J. P. Hansen, and E. J. Meijer, "Accurate effective pair potentials for polymer solutions," J. Chem. Phys. **114**, 4296–4311 (2001).

[85]J. Dautenhahn and C. K. Hall, "Monte Carlo simulation of off-lattice polymer chains: Effective pair potentials in dilute solution," Macromolecules **27**, 5399–5412 (1994).

[86]A. A. Louis, P. G. Bolhuis, and J. P. Hansen, "Mean-field fluid behavior of the Gaussian core model," Phys. Rev. E **62**, 7961–7972 (2000).

[87]R. Finken, J. P. Hansen, and A. A. Louis, "Phase separation of penetrable core mixtures," J. Stat. Phys. **110**, 1015–1037 (2003).

[88]A. J. Archer and R. Evans, "Binary Gaussian core model: Fluid-fluid phase separation and interfacial properties," Phys. Rev. E **64**, 041501 (2001).

[89]A. J. Archer, "Dynamical density functional theory: Binary phase-separating colloidal fluid in a cavity," J. Phys.: Condens. Matter **17**, 1405–1427 (2005).

[90]A. J. Archer, C. N. Likos, and R. Evans, "Soft-core binary fluid exhibiting a λ-line and freezing to a highly delocalized crystal," J. Phys.: Condens. Matter **16**, L297 (2004).

[91]A. J. Archer, "Dynamical density functional theory: Phase separation in a cavity and the influence of symmetry," J. Phys.: Condens. Matter **17**, S3253–S3258 (2005).

[92]M. Schmidt, "Power functional theory for many-body dynamics," Rev. Mod. Phys. **94**, 015007 (2022).

[93]P. J. Flory and W. R. Krigbaum, "Statistical mechanics of dilute polymer solutions. II," J. Chem. Phys. **18**, 1086–1094 (1950).

[94]S. Milster, A. Darwish, N. Göth, and J. Dzubiella, "Synergistic chemomechanical dynamics of feedback-controlled microreactors," Phys. Rev. E **108**, L042601 (2023).

25 September 2024 08:07:06